Oxygen ordering in $YBa_2Cu_3O_{6+x}$ using Monte Carlo simulation and analytic theory

Dan Mønster,[1] Per-Anker Lindgård,[2] and Niels Hessel Andersen[2]
[1]*UNI-C, Danish Computing Centre for Research and Education, Olof Palmes Allé 38, DK-8200 Århus N, Denmark*
[2]*Materials Research Department, Risø National Laboratory, DK-4000 Roskilde, Denmark*
(Received 27 February 2001; revised manuscript received 28 June 2001; published 26 November 2001)

We have simulated the phase diagram and structural properties of the oxygen ordering in $YBa_2Cu_3O_{6+x}$ testing simple extensions of the asymmetric next-nearest-neighbor Ising (ASYNNNI) model. In a preliminary paper [Phys. Rev. B **60**, 110 (1999)] we demonstrated that the inclusion of a single further neighbor interaction gave results that could account for several hitherto unexplained structural observations. In this paper we make an extensive study showing that these results are robust against further extensions. Additional inclusion of three-dimensional or infinite range interactions does not obviate the finding of the following results: the existence of ortho-III, ortho-V, and ortho-VIII phase correlations; suppression of the ortho-I–ortho-II transition temperature relative to that of the tetragonal–ortho-I transition; no ortho-II Bragg peaks, but a crossover from Lorentzian toward Lorentzian squared line shapes; and a finite average chain length even at low temperatures. Simulations with the extended (ASYNNNI) model yield a realistic picture of the oxygen order of importance for the understanding of the hole doping. The experimental facts are consistent with a low temperature structure broken up on a nano scale into box-like domains and anti-domains of typical average dimension $(10a,30b,2c)$. Theory and model simulations demonstrate that the distribution of such domains causes deviations from Lorentzian line shapes, and not the Porod effect. Analytic theory is used to estimate the effect of a range of values of the interaction parameters used, as well as the effect of an extension to include infinite ranged interactions. In the experiments a large gap is found between the onset temperatures of the ortho-I and ortho-II orders at $x=0.5$. This cannot be fully reproduced in the simulations. The simulations yield a quite symmetric phase diagram around $x=0.5$ with respect to the low temperature phases, whereas experimentally it has not been possible to detect such phases for small-x values.

DOI: 10.1103/PhysRevB.64.224520 PACS number(s): 61.43.Bn, 05.50.+q, 74.72.Bk

I. INTRODUCTION

$YBa_2Cu_3O_{6+x}$ is one of the prototypical materials exhibiting high-temperature superconductivity. Therefore, a detailed investigation and understanding of the oxygen ordering are crucial as a basis for finding the mechanism of the phenomenon.

It is well known that incompletely filled CuO_x layers in the $YBa_2Cu_3O_{6+x}$ (YBCO) type of high-T_c superconductors act as electron acceptor units, and that hole doping into the superconducting CuO_2 planes is governed by the formation of O-Cu-O chains. Unlike some other high-T_c materials, where the acceptor units are insulating, O-Cu-O chains become metallic when they exceed a certain length and act as electron acceptors.[2] It is therefore generally accepted that the oxygen ordering and associated metallic behavior of the chain structure contribute to the superconducting properties. This is corroborated by calculations of the electron band structure, which show that both the plane and the chain bands contribute to the Fermi surface.[3,4]

A precise picture of the chain structure oxygen ordering is therefore important for an accurate determination of the electronic structure and the superconducting properties of YBCO. Direct experimental evidence of the relation has been established from quench studies where the time evolution of the orthorhombic strain could be correlated with that of T_c.[5] This relation, and early phenomenological relations between experimental T_c data and simulations of the oxygen ordering,[6,7] indicate that the formation of ordered domains is essential, but it has never been proven directly. In this paper the domain structure will be critically investigated by model simulations and by analytic means.

The obvious need for detailed structural information on a local scale has motivated numerous experiments aimed at determining the oxygen structure by electron microscopy,[8–11] x-ray and neutron scattering,[12–17] and NMR.[18] Diffraction experiments give only indirect information about the local real-space ordering properties, and the information from NMR is restricted to the oxygen coordination number of the Cu. Furthermore, the experiments clearly showed that the structural ordering remains of finite size even in high purity crystals, and it is strongly dependent on the oxygen composition as well as on the thermal annealing treatment. To interpret available information correctly, it is important to make accurate Monte Carlo simulations which will reproduce the pertinent details observed in scattering experiments, and which are simultaneously able to give the corresponding real space information. We believe that our simulations accomplish a significant further step toward this than previous model studies.[3,19–39]

Diffraction studies of YBCO clearly showed the existence of superstructures characterized by O-Cu-O chains that are aligned along the *b* axis and ordered with different periodicity along the *a* axis.[8,9,11,11–17] The interactions between the oxygen atoms can predominantly be described by their Coulomb repulsion (resulting in the parameters called V_1 and V_3), except for the interaction along the chains which is influenced by hybridization via the Cu ions (resulting in the parameter called V_2). Detailed microscopic theories[2,20,21,26,27] suggest, in particular, that the V_2 param-

eter could be dependent on the structure, i.e., the chain length of the formed chains, and thus on the temperature T as well as the composition x. Including this would go beyond the description possible by the simple lattice model, called the asymmetric next-nearest-neighbor Ising (ASYNNNI) model,[28] which has fixed interaction parameters V_1, V_2, and V_3.

The merit of the model is its simplicity, and it has been shown[30,38] to account accurately for the main structural transition between the tetragonal to ortho-I structures[40] and the prediction of the observed ortho-II superstructure with chains separated by two lattice units a. However, a number of additional experimental findings[12–17] cannot be accounted for. Of particular relevance to the chain length discussion is that no long-range order of the ortho-II phase is observed, and that the ortho-II transition occurs at significantly lower temperatures than predicted by the ASYNNNI model near $x=0.5$. Also the observed trend toward an almost squared Lorentzian line shape[15] in place of a sharp Bragg peak indicates the formation of a microdomain structure with finite chain length. The ASYNNNI model also falls short of explaining the observation of higher order superstructures with periodicities of $3a$ (ortho-III), $5a$ (ortho-V), and of apparently incommensurate structures (ortho-VIII), which have been observed by electron microscopy,[8–11] and recently identified as genuine bulk structures by synchrotron and neutron scattering investigations.[17] To describe this, long-ranged interactions between the oxygen atoms might be needed.

In this paper we stick to the basic assumption of the ASYNNNI model: the T- and x-independent interaction parameters. We wish to test to what extent the model reasonably, but minimally, extended can account for the observed data, or whether deeper modifications are called for. We present results for the superstructure ordering obtained from Monte Carlo simulation studies based on an extension of the two-dimensional (2D) ASYNNNI model[28] that includes one additional effective repulsive interaction V_5 between oxygen atoms that are $2a$ apart and not bridged by copper atoms.[41] Preliminary studies of this model have shown that V_5 interaction stabilizes the ortho-III by construction where it is expected, but surprisingly it also accounted for other experimental observations.[1] Here we extend this work considerably, and present a detailed analysis of the superstructure ordering properties and the phase diagram that result by adding V_5 to the ASYNNNI model with emphasis on structure factors pertinent to comparison with experimental diffraction data. We further test that the results and understanding of the structures remain unchanged when the simulations include a small 3D interaction V_4 between oxygens in neighboring planes.

II. MODEL

Long-range, albeit screened, interactions between oxygen atoms are expected[22,23,26,27,29] on the basis of the Coulomb interaction. These may in principle be calculated and included in the model at the cost of an extensive enhancement of the computational effort. Furthermore, beyond a certain range the interactions are small and redundant because they come into play only at temperatures where the oxygen ordering kinetics is effectively frozen. We have found that by introducing only one extra in plane parameter to the ASYNNNI model one can account for most of the outstanding problems relative to the experimental electron, neutron, and x-ray scattering data. The effect of longer range interactions is discussed using an analytic theory.

The extended ASYNNNI model for the oxygen ordering in YBCO that we have studied by Monte Carlo (MC) simulation technique is:

$$\mathcal{H} = -V_1 \sum_{\langle \mathbf{r}\mathbf{r}' \rangle}^{\mathrm{NN}} \sigma(\mathbf{r})\sigma(\mathbf{r}') - V_2 \sum_{\langle \mathbf{r}\mathbf{r}' \rangle}^{\mathrm{NNNCu}} \sigma(\mathbf{r})\sigma(\mathbf{r}') - V_3 \sum_{\langle \mathbf{r}\mathbf{r}' \rangle}^{\mathrm{NNNV}} \sigma(\mathbf{r})\sigma(\mathbf{r}') - V_4 \sum_{\langle \mathbf{r}\mathbf{r}' \rangle}^{\mathrm{NNPl}} \sigma(\mathbf{r})\sigma(\mathbf{r}') - V_5 \sum_{\langle \mathbf{r}\mathbf{r}' \rangle}^{\mathrm{NNN2V}} \sigma(\mathbf{r})\sigma(\mathbf{r}'). \quad (1)$$

Here $\sigma(\mathbf{r})=1$ or 0 depending on whether the site $\mathbf{r}$ is occupied or not and the sums run over all oxygen pairs $\langle \mathbf{r},\mathbf{r}' \rangle$, which are nearest neighbors (NN), next nearest neighbors bridged by Cu (NNNCu), and not bridged by Cu (NNNV). The corresponding interaction parameters are V_1, V_2, and V_3. The extra interaction parameter V_5 couples pairs not bridged by a Cu and $2a$ apart (NNN2V), and V_4 represents interaction between neighboring planes (NNPl). This was not considered in our preliminary work.[1] Variations of this model were studied previously by the cluster variation method, and analytically based on the assumption of very (infinitely) long O-Cu-O chains.[25,29,30,32–36] These studies are therefore less suited for an analysis of the local structural properties observed experimentally.

From previous studies of the ASYNNNI model,[38] where simulations were compared to experimental data, the interaction parameters were determined as $V_1/k_B=-5430$ K, $V_2=-0.36V_1$, and $V_3=0.12V_1$, where k_B is Boltzmann's constant. The values are in good agreement with the results obtained by *ab initio* electron band-structure calculations,[42] and this is not violated by the small scaling of V_1 needed when small nonzero V_4 and V_5 are included. The relative magnitudes of all the interactions are in agreement with observed line widths of the structure factor, which also requires $V_4 \approx -0.02V_1$, as used previously[38] in a simulation without V_5. From estimates based on a screened Coulomb potential[25] we have found that $V_5/V_1=0.02\pm0.02$ should be a reasonable interval for the investigations. Such values of V_5 makes it play a role only at temperatures where the O-Cu-O chains are basically already formed.

The introduction of the V_5 interaction actually stabilizes the ortho-III phase (near $x=1/3$ and 2/3) "by construction," but it turns out to explain more than was meant by its design. The need for including all interactions of a screened Coulomb potential is therefore limited and probably not important for describing the experimentally observed phases, as discussed below. However, it may be important to include other long-range interactions such as strain effects. An obvi-

ous effect of strain fields is that coexistence of aligned antiphase domains is favored over that of perpendicular domains. In the experimental situation a dominant chain alignment is introduced at the tetragonal to ortho-I (T-I) transition. In the ASYNNNI model studies based on Eq. (1), the two types of domains are fully equivalent. However, as a (favorable) consequence of the finite-size samples used in the simulations, the coexistence of perpendicular domains is suppressed due to the advantage of creating continuous chains. Hence parallel antiphase domains are favored in a way similar to the effect of a unidirectional strain.[39] From examinations of direct space images obtained in our present studies, we consequently find only few examples of coexisting perpendicular domains, and they are hardly important for the calculated structure factors. On the other hand, it is very important to simulate samples of sufficient size and with a sufficient number of independent ensemble members, in order to be able to represent a sufficiently large distribution of the parallel anti phase-domains, as discussed below.

Attempts to include strain effects directly have been made by use of mean-field-like simulations.[37] These and other studies of the extended ASYNNNI model[33,34] yield the ortho-III structures, but neither the ortho-V nor ortho-VIII structures. A detailed description of strain effects, and other mesoscopic features as twin formation, is beyond the present goal. Our simulations are more accurate than the mean-field simulations with respect to the phase diagram and the local structures (inside a twin domain). Due to the reciprocal space method used in Ref. 37 a wavelike structure with very short chains is proposed. This is not found in any real space simulations.

In very recent MC simulations[43] the focus was on the original ASYNNNI model with strain effects included as a chain length penalty. The main results are that finite chain lengths and twin domains are formed by construction, the tetragonal to orthorhombic transition temperature is significantly reduced, and no new phases result from the strain.

III. MONTE CARLO DETAILS

All Monte Carlo simulations have been carried out using Kawasaki dynamics at fixed particle number and thus fixed oxygen concentration x. We have used a multimember ensemble approach, which ensures that we obtain independent configurations when sampling our observables. This is particularly important at the lowest temperatures where the system tends to freeze, and the single-member ensemble approach yields very poor statistics due to the fact that the states that are sampled are practically identical. Simulating a multimember ensemble is a task which is trivial to do in parallel, since it basically consists in performing the same simulations with different initial conditions and then average the results of the individual simulations afterwards. We have typically used ensembles with 32 independent members for the 2D simulations and eight-member ensembles for the 3D simulations. The predominant system size used in the simulations is 128×128 (2D) and $128\times128\times32$ (3D). Periodic boundary conditions have been imposed in all spatial dimensions.

The 2D MC simulations are performed as described below. At a given concentration the system is prepared with oxygen atoms in randomly chosen positions. We simulate the quenching and gradual cooling of this system as a function of the reduced temperature $T^*\equiv k_BT/|V_1|$ as follows. The initially random state is quenched to a temperature somewhat above the ordering temperature. At this temperature the system is allowed to equilibrate for a number of Monte Carlo steps per site (MCSS)—typically 5000 MCSS. In our approach a Monte Carlo step consists of selecting an oxygen atom (particle) and a vacancy (hole) at random and then use the Metropolis algorithm to decide whether or not to interchange the particle-hole pair, i.e., we allow nonlocal jumps. This is not meant to model the actual physical process, but rather is chosen as an efficient Markov process to ensure that equilibrium is reached rapidly. After equilibration we sample the structure factor $S(\mathbf{q})$, the energy, the specific heat and the concentration of l-fold coordinated Cu atoms, c_l. Each sample is separated by a number of MCSS—typically 10. After the specified number of configurations (typically 100) have been sampled the temperature is reduced and the process of equilibration and sampling is repeated for the new temperature. In this way we perform stepwise cooling, equilibration, and sampling in equal temperature steps, until a desired minimum temperature—typically $T^*=0.05$—has been reached. At each temperature the results from different members of the ensemble are averaged.

This scheme was found optimal for studying the ordering process of structural phases with frozen domain structures, and it is different from previously used strategies,[38,39] where a single-member ''ensemble'' was averaged over a long-time series instead. In particular, the present method allows a study of the average domain structure that the system assumes. Importantly, the approach toward single domain states for low temperatures proceeds exceedingly slowly in the simulations.[33,34] This is also observed in the experimental situation partly due to slow oxygen diffusion at low temperatures, which effectively freezes the structures at a temperature of ~325 K or at $T^*\sim0.06$. However, the simulations show that the highly anisotropic models favor creation of straight, stacking-fault-like, domain walls, which have no tendency to move under curvature driven domain growth. A previous Monte Carlo study of the domain growth kinetics has shown that it may result in logarithmicly slow growth.[44]

The 2D Monte Carlo simulations were performed as function of the reduced temperature T^* for two different values of the V_5 parameter: $V_5=0.02V_1$ and 0.04 at 23 and 22 different compositions in the interval $0.2\leqslant x\leqslant0.9$, respectively. The above description of the 2D simulation scheme is applicable to 3D simulations as well, if these are considered to be coupled 2D simulations. This picture is valid since particle-hole interchange is confined to take place within a given layer of the three-dimensional system.

The 3D simulations were performed for nine different compositions between $0.25\leqslant x\leqslant0.75$ and for $V_4=-0.02V_1$, and a few runs with $V_4=-0.01V_1$: at $x=0.25$ and at 0.5 in order to determine the optimal value in presence of the finite $V_5=0.02V_1$. The phase diagram was determined at $x=0.25$, 0.333, 0.40, 0.5, 0.60, and 0.66 using samples of size

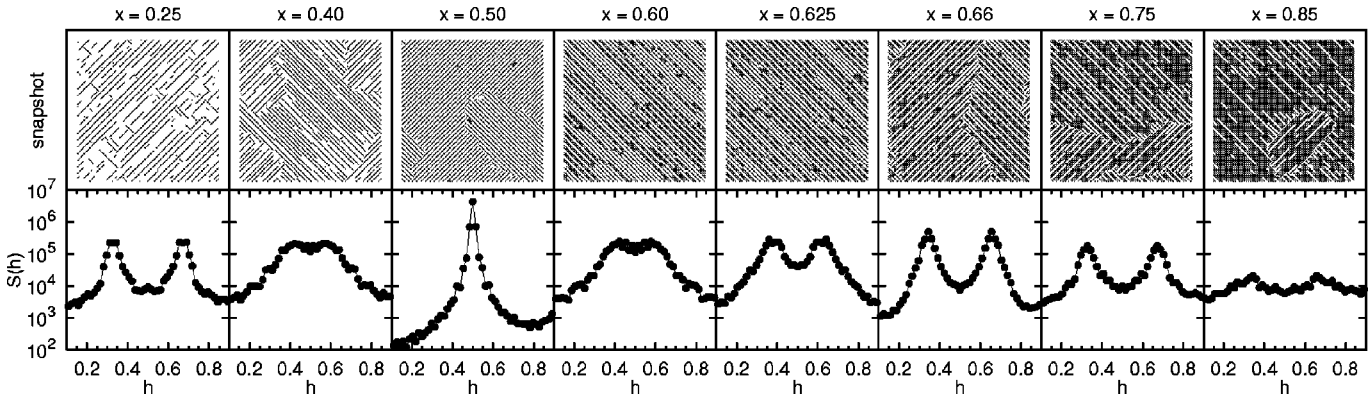

FIG. 1. Lower panels: the 2D-simulated structure factor for selected x values from $x=0.2$ to $x=0.85$ for $V_5=0.02V_1$ at $T^*=k_BT/|V_1|=0.06$ for $\mathbf{q}$ along $\{h0\}$. Note the absence of a Bragg peak. Above: corresponding snapshots (chosen to show perpendicular domains); black symbols indicate oxygen positions. Note the remaining domain structure.

$64\times64\times32$ and an ensemble of eight independent systems. At $x=0.25$, 0.375, 0.5, 0.64, and 0.75 we used the larger samples of size $128\times128\times32$ and also ensembles with eight independent members in order to obtain a sufficiently accurate determination of the structure factor.

IV. RESULTS OF THE 2D SIMULATION

In this section we present the results of the structural properties of oxygen ordering in YBCO found for $V_5=0.02V_1$ and 0.04 at the different values of x and T^*. In the analysis and presentation of the structure factor data for convenience we use the reduced coordinates $\mathbf{q}^*=(h,k)=(q_h/a^*,q_k/b^*)$, where a^* and b^* are the reciprocal lattice constants. For symmetry reasons there is no distinction between the h and k directions in the ASYNNNI model, and on average the superstructure intensity is the same along the $(h,0)$ and $(0,k)$ directions. We shall throughout present the superstructure ordering vector as being at h_i along the h direction, although the actual $S(\mathbf{q}^*)$ data represent an ensemble average over both directions. Similarly averaged, we will describe the transverse scans through the superstructure peaks at $q^*=h_i$ by k. The q^*-space data are fitted with the function

$$S(q^*)=\sum_i \frac{A_i\kappa_i}{[(q^*-q_i^*)^2+\kappa_i^2]^{\phi}}, \tag{2}$$

where $q^*=h$ and $q_i^*=h_i$ for an a h scan at $k=0$, and $q^*=k$ and $q_i^*=0$ for a k scan at h_i. κ_i is the inverse correlation length and A_i is the amplitude. We allow for a line shape as a Lorentzian raised to a power $\phi\neq1$, as expected for scattering from distributions of small domains with sharp boundaries.

In the following we shall first discuss the behavior for $V_5=0.02V_1$. The results obtained for $V_5=0.04V_1$ are qualitatively very similar to those for $V_5=0.02V_1$, except that considerable signs of the short-range order of ortho-III is found in the ortho-I phase at $x=0.5$. Since this is not seen experimentally, we conclude that this value of V_5 is too high. However, to show the systematics introduced by varying the longer range repulsion parameter, we also present data for $V_5=0.04V_1$, and discuss them along with other values: $V_5=0.01V_1$ and $V_5=0$.

A. Reciprocal and real space information

In Fig. 1 we show, for $T^*=0.06$ and several values of x the simulated structure factors, $S(\mathbf{q}^*)$ on a logarithmic scale for the wave vector $\mathbf{q}^*$ in the $(h,0)$ direction. It should be emphasized that the major intensity of the ortho-V and ortho-VIII peaks are expected to be at $h_5=2/5$ and 3/5, and at $h_8=3/8$ and 5/8, respectively. $S(\mathbf{q}^*)$ was also evaluated and analyzed for $\mathbf{q}^*$ in the k direction at chosen h_i values. Two examples for $x=0.4$ and 0.5 and T^* at the transition temperature are shown in Fig. 2.

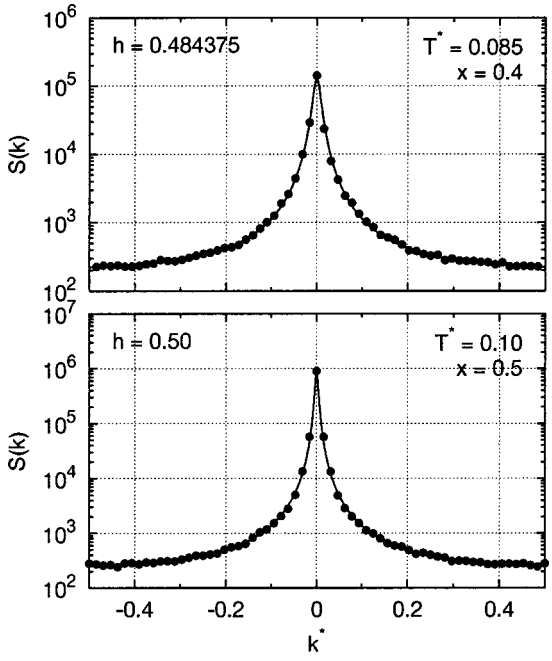

FIG. 2. Line shapes of the k scans through $q^*=0.5$ for (a) $x=0.4$ and (b) for $x=0.5$ and $T^*=T_Q^*$. The line is a fit to a Lorentzian line shape.

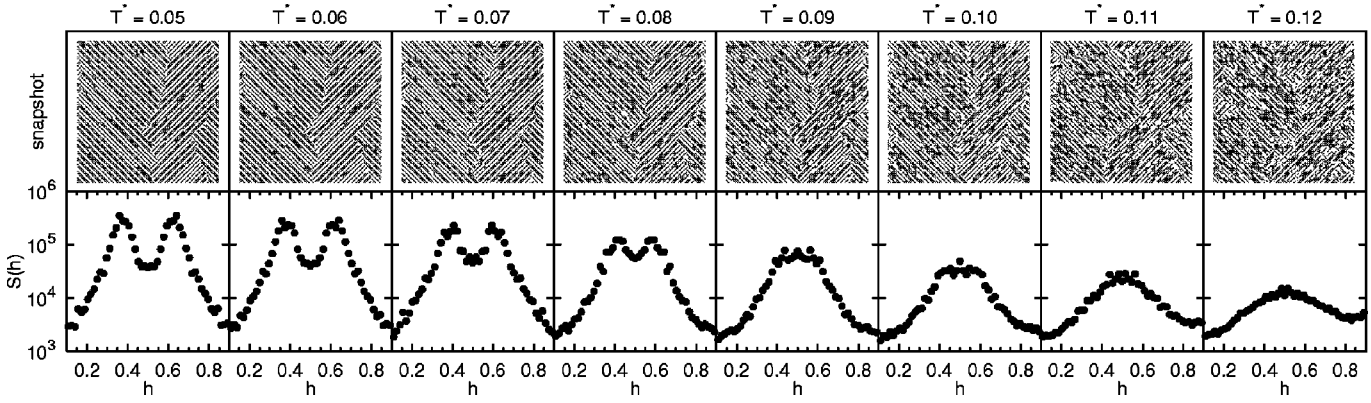

FIG. 3. Lower panels: temperature evolution of the 2D-simulated structure factor for $x=0.625$ for $V_5=0.02V_1$ from $T^*=k_BT/|V_1|=0.05$ to $T^*=0.12$ for $\mathbf{q}$ along $\{h0\}$. Note the onset of enhanced short range order at $T^*\sim 0.09$. Above: typical corresponding snapshots; black symbols indicate oxygen positions.

The $S(\mathbf{q}^*)$ profiles provide characteristic reciprocal space signatures of the various phases for increasing composition x and at the relatively low temperature $T^*=0.06$. It is evident, and very interesting, that no long-range order is developing. This feature has been a longstanding puzzle in experimental investigations on YBCO, and has been attributed to effects of random fields from impurities.[15] It is clear that the ortho-II peak at $h_2=0.5$ for $x=0.5$ splits up into two peaks for both higher and lower x values. This constitutes the scattering signatures for the higher order ortho-N structures, also found experimentally. In both situations it is found that the ortho-N structures represent highly correlated structures, without being true thermodynamic phases, since no Bragg peaks are found, and hence no true long range order exists. The MC simulations allow a representation of the corresponding real space pictures, shown in the upper panel of Fig. 1. These are excerpts of the simulated 128×128 cells, and they are of course only single snapshots. To obtain the shown reciprocal space information one needs an average over the 32 different ensemble members, further averaged over ten consecutive configurations separated by ten MCSS. With this in mind it is possible to judge that most of the structures consist of fairly small domains in which there exists considerable disorder in the form of mixed phases of various ortho-N patterns. As a result the q-space peaks may be broad and shifted relative to the expected pure h_N positions, thus inviting to an interpretation as incommensurate structures. These peaks cannot be decomposed into a sum of even broad peaks characteristic of different pure ortho-N phases. The snapshots give an idea of how the corresponding structure should be understood. In the simulations we find, as mentioned above, a small fraction of the ensemble members to have perpendicular domains in addition to simple antiphase domains. In real YBCO we expect the former to be even further suppressed—if not totally removed by the orthorhombic strain effects. However, the finite size of the simulations does effectively reduce the probability that such domains are present in more than just a few of the ensemble members, and hence in this respect mimic the effect of strain, as discussed previously.

Figure 3 shows the evolution with temperature of one such structure at $x=0.625$. The lower panel shows the ensemble averaged structure factor $S(h)$, and the upper panel shows snapshots of the corresponding real-space structures. At the lowest temperatures this might be interpreted as an ortho-VIII structure with $h_8=3/8$. In Fig. 4 we show the temperature variation of the characteristic peak position h_i for $x=0.375$ and 0.625. There are symmetric peaks at h_i and $1-h_i$, as can be seen in Figs. 1, and 3, but for clarity we show only one set in Fig. 4. With decreasing temperature the peaks move continuously in position and with an intensity that increases and a linewidth that sharpens rapidly at a given temperature (indicated by arrows). Here, as when analyzing the experimental data, we shall define this temperature as the transition temperature between the ortho-I structure and the ortho-N structures, $T_Q^*=T_c^*(\text{I-}N)$. However, it is clearly demonstrated in Fig. 3 that short-range correlations of ortho-N type exist far up in the ortho-I phase. The presence of an ortho-III phase is indicated by peaks in the structure factor and a periodicity 1/3 with peaks at $h_3=1/3$ and 2/3. This is clearly seen in Fig. 1. This structure is directly stabilized at $x=1/3$ and 2/3 even by a repulsive V_5. However, it is by no means clear that the addition of the V_5 parameter will give rise, for example, to the ortho-V structure, since an extra even longer range interaction might be needed to resolve a degeneracy between ortho-V and other similar phases. Nevertheless we have observed clear indications of ortho-V do-

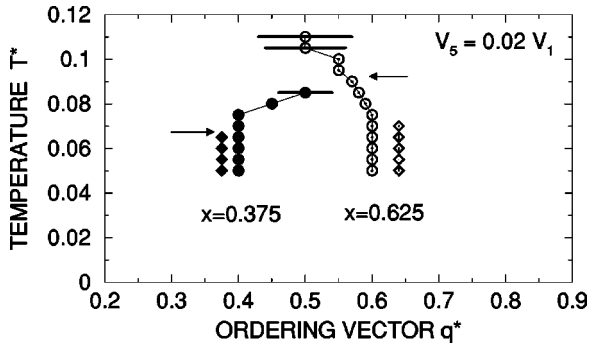

FIG. 4. Temperature dependence of the peak position at $x=0.375$ (filled symbols) and $x=0.625$ (open symbols). The presence of a mixed phase is indicated by the appearance of two sets of symbols, one for each of the distinguishable peaks in $S(\mathbf{q})$. The transition temperatures T_Q^* are indicated by the arrows.

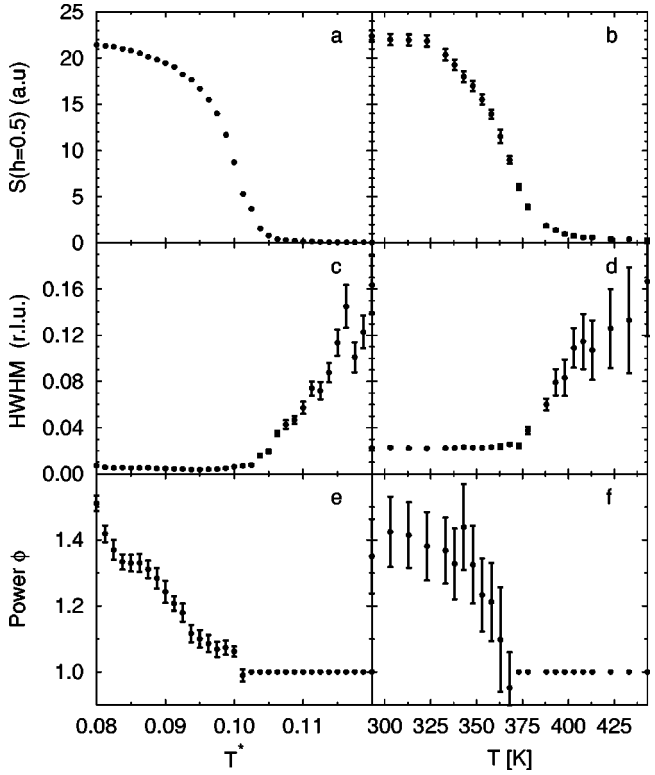

FIG. 5. (a) The peak intensity of the 2D-simulated structure factor for a 128×128 system at oxygen composition $x=0.50$ vs temperature. (b) Same, obtained experimentally (Ref. 17). (c) The simulated temperature dependence of the peak half-width at half-maximum (HWHM) (Δh^*), in reciprocal lattice units ($2\pi/a$). (d) Same, obtained experimentally (Ref. 17). (e) The fitted Lorentzian power ϕ. (f) Same obtained experimentally (Ref. 17). A close similarity between the experimental and simulated properties is evident.

mains both in the structure factor data for x near 0.4 and 0.6, and in snapshots of system configurations as shown in Fig. 1. If the system had established long range ortho-V order the major peaks in the structure factor would be at $h_5=2/5$ and $h_5=3/5$, but due to the random mixture of III and V chain sequences, which one may call an ortho-VIII phase (with $h_8=3/8$ and $h_8=5/8$), the peaks are shifted away from these values. This is rationalizing the seemingly incommensurate phases.[11,17]

B. Line shape

The line shapes along k and h for $x\sim0.5$ are well resolved and described by a Lorentzian for $T^*\geqslant T_c^*$(I-II). In contrast we obtain significantly better fits to both h and k scans in the ordered phase using a Lorentzian raised to a power $\phi>1$. This is most clearly detected in the ortho-II phase where there is no peak overlap. Figure 5 shows the result of a peak analysis for $x=0.5$ as function of the reduced temperature T^*. In Fig. 5(a) we show the peak intensity as a function of temperature for the peak at $h_2=0.5$; it compares very well with the behavior of experimental data shown in Fig. 5(b). The half width at half maximum (HWHM) is shown in Fig. 5(c), again in good agreement with the experimental behavior in Fig. 5(d). We determine the transition temperature

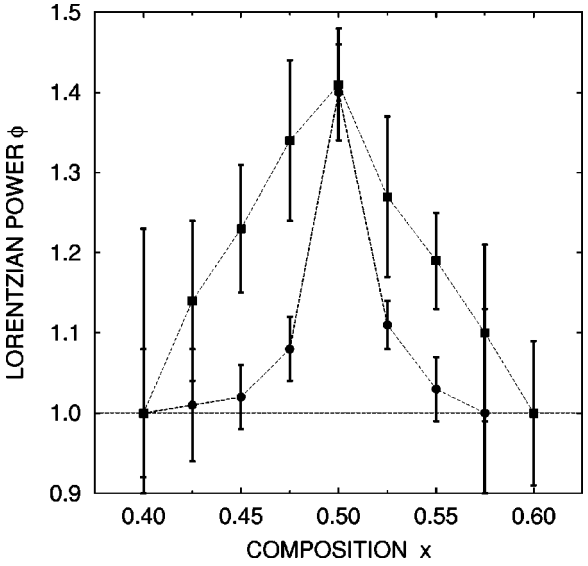

FIG. 6. The exponent ϕ for the fit to line shapes at $T^*=0.06$ using a Lorentzian to a power ϕ, at the x values shown. (●) are for h scans, and (■) for k scans.

T_c^*(I-II) by inspecting the combined behavior of the increase in peak intensity and the decrease in width as T^* is reduced. Similar analyses were done for all the simulated x values. Below T_c^* there is no Bragg peak and the width of the diffuse scattering does not increase [Figs. 5(c) and 5(d)], in either the simulations or in the experiments, as would be expected for regular continuous phase transitions. The reason for this is the freezing of the rather small-scale domain structure. In Fig. 5(e) we show that the line shape in the h direction at $(\frac{1}{2},0)$ is described with a ϕ that increases toward $\phi=1.5$ below T_c^*. A similar behavior in the experimental data is displayed in Fig. 5(f).

The typical interpretation of such deviations from Lorentzian line shape is the building up of sharpening domain walls. For a low-density distribution of equal-size spherical particles (domains) with *sharp boundaries*, $S(q^*)$ follows Porod's law, i.e., it has $\phi=(d+1)/2$, where d is the dimensionality. However, the basis for the Porod model is, by examination of the snapshots, clearly not fulfilled. There are no separate spherical domains. The model is therefore not directly relevant for the YBCO system. An alternative model will be discussed below in connection with the 3D simulations.

Summarizing, in two dimensions for x near 0.5 the line shape in neither the h nor the k scans can be well fitted with a Lorentzian shape at $T^*=0.05$, whereas using a $\phi>1$ provides a much better fit. As shown, the exponent ϕ increases gradually from the value of 1 at the transition temperature. The variation with x of the obtained $\phi>1$ is shown in Fig. 6. Some of the corresponding line shapes and fits are shown in Fig. 7. Outside the x interval where multiple peaks occur in the h scans, the line shape is not sufficiently well determined with respect to $\phi\neq1$, and we have used simple Lorentzians in our fits. This provides perfect fits to all k scans. Hence ϕ is probably 1 outside the x interval shown in Fig. 6.

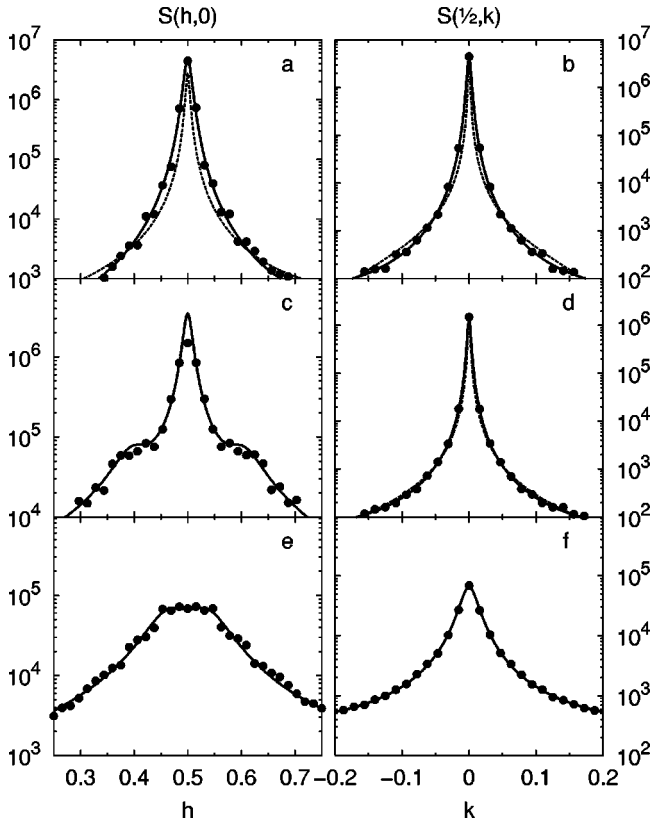

FIG. 7. Corresponding fits yielding the powers shown in Fig. 6. Full lines: fits to the Lorentzian to a power with $\phi > 1$. Broken lines (where shown): fits for $\phi = 1$. (a) and (b) $x = 0.5$ and $T^* = 0.05$. (c) and (d) $x = 0.55$ and $T^* = 0.05$. (e) and (f) $x = 0.60$ and $T^* = 0.10$. All with $V_5 = 0.02V_1$.

C. Chain length

In Fig. 8, for various values of x, and $V_5 = 0.02V_1$, we show the obtained concentration c_l of $Cu^{(l)}$ atoms with l nearest oxygen neighbors (including two apical ones) for $T^* = 0.12$ and $T^* = 0.05$, respectively. The system size is 128×128. The average chain length $\langle L \rangle$ is simply[21] $\langle L \rangle = 2x/c_3$; it can also be found directly from the length distribution. First we note that c_l and $\langle L \rangle$ vary smoothly with x, although with a small dip at x slightly higher than $x = 0.5$. This behavior is in qualitative agreement with the experimental data[18] (error bars were not given). The variation with x is in the different model and simulation by Haugerud and Uimin[21] found to be somewhat larger, but for $x = 0.5$ and $V_5 = 0$ we find exact agreement between their results and ours. Thus at $x = 0.5$ the chain length, surprisingly, is independent of the modification of the ASYNNNI model considered in Ref. 21. For $x = 0.5$ the experimental data for c_l at $T = 450$ K (Ref. 18) give $c_3 = 0.19$ or $\langle L \rangle = 5.3$. They also give $c_4 = 0.44$ and $c_2 = 0.37$. The difference may indicate the size of the error bars, since at $x = 0.5$ one would expect $c_4 = c_2$.[21] Our value at the corresponding temperature $T^* = 0.08$ is $\langle L \rangle = 7.8$ for $V_5 = 0.02V_1$, This in reasonable agreement with the experimental value. In particular, it is relatively small compared to that expected for well ordered systems.

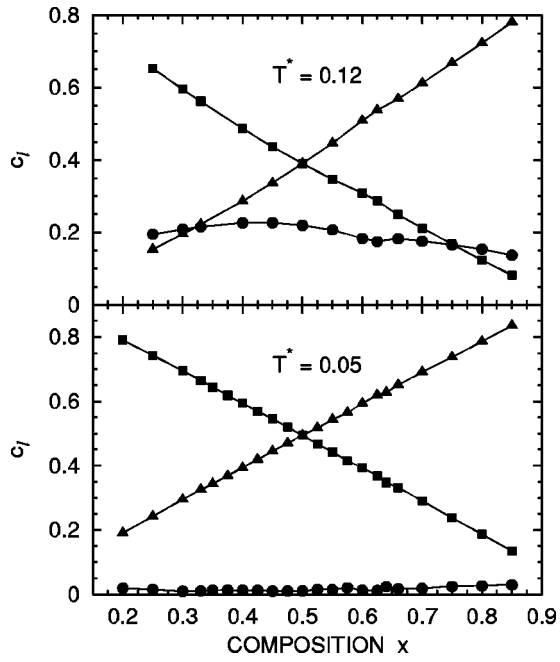

FIG. 8. The concentration c_l of l-coordinated $Cu^{(l)}$ atoms (including apical oxygen) vs x for $T^* = 0.12$ and $T^* = 0.05$. Square: twofold coordination; circle; threefold coordinations; triangle; fourfold circle: coordination. The average chain length is $\langle L \rangle = 2x/c_3$. Simulated for 128×128 2D systems. Note that c_3 and hence $\langle L \rangle$ are finite even at the lowest temperatures. Lines are guides to the eye.

The effect of a 3D coupling V_4 on the phase diagram can be accounted for by reducing $|V_1|$ by 26%, judged from the simulated 2D and 3D $T^*_{\text{I-II}}$ at $x = 0.5$. On the other hand, the effect on the ordering, and hence on c_l, in adjacent planes should be negligible. When including the effect of V_4 in this way we obtain $\langle L \rangle = 6.2$, in still better agreement with the experimental value. A direct simulation of the average length is difficult in the 3D simulations, since the tendency to order is enhanced. We are not able to use larger in-plane system sizes, since we also need to have sufficiently many ensemble members and planes stacked to reproduce the 3D effects. Unfortunately, the chosen systems cannot sustain a realistic chain length distribution.

Surprisingly, it is found that even the weak 3D coupling does cause a greater tendency to order within the planes as well as that between the planes. This is probably because this ordering is not prohibited by frustration effects. Generally, it can be concluded that the introduction of a finite V_5 produces a quite small $\langle L \rangle$ also for smaller T^*; see Fig. 8.

D. Phase diagram

Based on our data and method of analysis described above it is possible to construct a phase diagram in the (x, T^*) plane. This is shown in the lower panel in Fig. 9(c) for $V_5 = 0.02V_1$ and in Fig. 10(c) for $V_5 = 0.04V_1$. The previously determined phase boundary for the pure ASYNNNI model with $V_5 = 0$ is shown as a dotted line on both graphs. A dramatic change is noticeable upon introduction of a finite V_5.

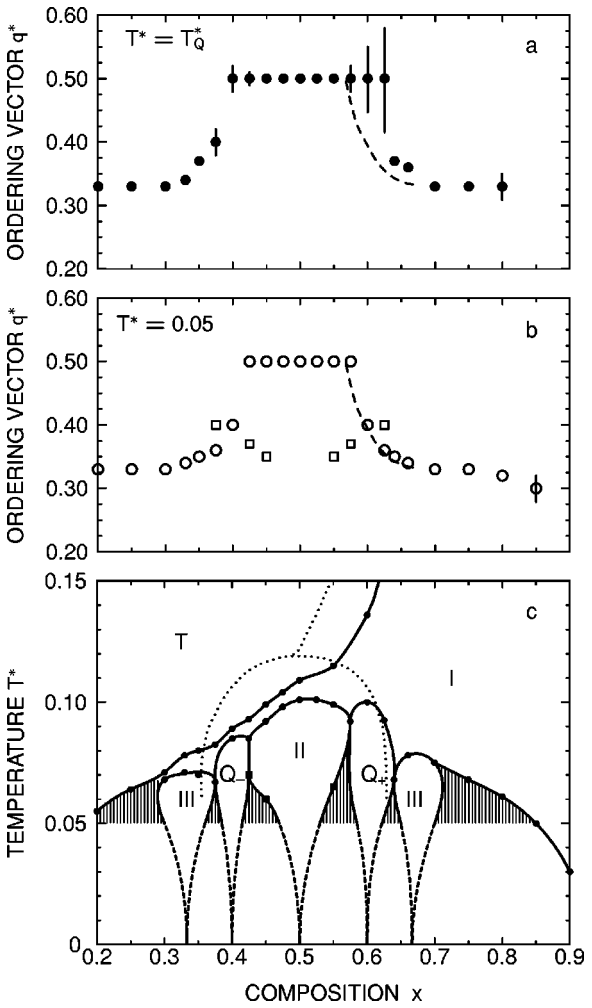

FIG. 9. Data for $V_5 = 0.02V_1$. (a) The simulated ordering q^* values (●) at the onset temperature $T^* = T_Q^*$, and (b) (○) at the lowest temperature $T^* = 0.05$. The vertical bars indicate the extent of the peak plateau; two symbols at the same x indicate mixed phase. Thin dashed lines show the theory of Khachaturyan and Morris (Ref. 49). (c) The resulting simulated phase diagram; (●) is the simulation data, and the full line is a guide to the eye. Black square indicates where two peaks, as signature of mixed phase (hatched) can be detected. Tentatively the Arnold tongues are continued to $T^* = 0$ (dashed lines) below the investigated region down to $T^* = 0.05$. The phase diagram obtained by the corresponding pure ASYNNNI model ($V_5 = 0$), using $V_2 = -0.36V_1$ and $V_3 = 0.12V_1$, is shown as a thin dotted line.

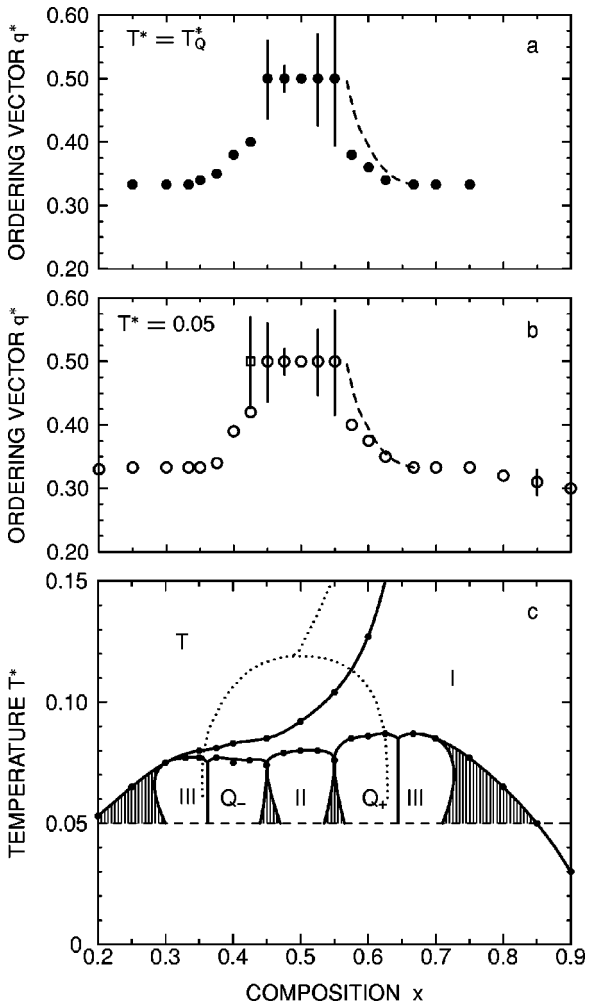

FIG. 10. Same as Fig. 9 for $V_5 = 0.04V_1$. According to the theory of Khachaturyan and Morris (Ref. 49) the Q_+ (and Q_-) regions may possibly extend fully down to low temperatures.

Figures 9 and 10 show that V_5 opens up a gap ΔT_G^* between the temperatures $T_{\text{T-I}}^*$ and $T_{\text{I-II}}^*$ of the tetragonal to ortho-I and the ortho-I to ortho-II transitions for a wide range of x values below $x = 0.5$. Such a gap was observed experimentally at $x = 0.5$,[15,17,40] but remained unexplained by the basic ASYNNNI model. For a proper estimation of the gap, we must include a small 3D coupling V_4 between the planes, the result of which is discussed below. In the simulations in Ref. 21, using a differently extended ASYNNNI model with a temperature dependent V_2, a small lowering of the ortho-II transition was discussed, but an opening of a gap was not demonstrated at $x = 0.5$.

Further, Figs. 9 and 10 show that the finite V_5 introduces wings of basically ortho-III order essentially outside the range of x values which shows ordering in the basic ASYNNNI model. In fact, it appears as if the introduction of the single longer range repulsion parameter is sufficient to restore ordering in a region which mean field theory would predict for ortho-II ordering within the basic ASYNNNI model, namely, as a parabola extending from $x = 0$ to 1. This is not too surprising, however, since here we are using the temperature at which short-range order rapidly sets in. This was previously[45] found to correlate well with the mean-field ordering temperature, although the true ordering temperature is strongly suppressed by fluctuations of disorder. At the boundaries are observed structures with variable ordering vectors, hence called Q_- and Q_+. For the lowest value, $x = 0.2$, and highest value, $x = 0.90$, the peaks are broad, weak and shifted toward $h_i = 0.3$ and 0.7. At these values of x the data hardly meet the criterion for being regarded as even a quasistructure using the present method. It is interesting that experiments on the high-x side found a phase diagram in very close agreement with the simulations, whereas at the low x side this terminates with ortho-II order at $x = 0.36$

without showing the simulated symmetric phases. At low temperatures, we observe a weak tendency to phase separation at the boundaries between neighboring phases. This is evident in the snapshots and in the development of (broad) characteristic peaks of both structures.

In the phase diagram shown on Fig. 9(c), the hatched areas represent regions with mixed phase, and the lines are guides to the eye through the determined points of transition temperatures $T_Q^* \pm \Delta T^*$. For most points the error bars are small $\Delta T^* \sim 0.002$, but unfortunately they are particularly large, $\Delta T^* \sim 0.005$, at $x \leqslant 0.25$ and $x \geqslant 0.85$ as well as at the eutectic points. However, even with this uncertainty there is evidence of stabilization of ''Arnold tongues'' of the principal ortho-II, -III, and V structures. This is not found in the basic ASYNNNI model with $V_5 = 0$. It is in good agreement with the experimental observations, but is rather surprising from the point of view of the simulations, since the extra V_5 could be regarded as just one out of many possible long-range repulsion parameters, and which does not directly stabilize the ortho-V order. This phase diagram is radically different from previously published diagrams calculated with a finite V_5, using, for example, cluster variation methods.[33,34] In these the ortho-I phase was found to penetrate down to $T^* = 0$ in place of the mixed phases. No such behavior has been experimentally observed. Ceder *et al.*[36] reproduced and discussed this result, and were able to remove the ortho-I penetration by including an effective 3D interaction between adjacent planes. They then found Arnold tongues of ortho-II and ortho-III order. The latter is displaced toward x larger than the ideal $x = \frac{2}{3}$, as we also find. This was also observed experimentally.[11,17] However, in place of our Q_+ phase (they only discussed $x \geqslant 0.5$) they only found a mixed region of ortho-II and ortho-III phases. They did use a value of $V_5 \sim 0.02V_1$ (there called V_4) identical to one of our values.

Although we have not been able to make simulations for $T^* < 0.05$ it is tempting to draw such Arnold tongues down to the respective pure values at $T^* = 0$, indicated by the dashed lines. This picture may not be true. Or at least, it may not be possible to drive neither the MC nor experimental systems to such equilibrium phases from high-temperature structures due to the slow oxygen kinetics.

E. Ordering vectors and comparison with theory

In Fig. 9(a) we show, for $V_5 = 0.02V_1$, the ordering vector values for the simulated range of oxygen filling x at $T^* = T_Q^*$, the temperature for the onset of the ordering. Figure 9(b) shows the ordering vector values at the lowest studied temperature $T^* = 0.05$. Similarly Figs. 10(a) and 10(b) show the behavior for $V_5 = 0.04V_1$. A vertical bar indicates that no clear peak is found, but only a broad flat maximum, the top width of which is indicated by the length of the vertical bar. A typical example of such a line shape is shown in Fig. 11 with a corresponding real space snapshot.

Let us discuss the $V_5 = 0.02V_1$ case first; see Fig. 9. It is evident that there exists a broad region around $x = 0.5$ for which the ortho-II structure ($h_2 = 0.5$) is found. The deviations from this is very symmetric for lower and higher values of x. First consider $T^* = T_Q^*$; see Fig. 9(a). Between $x = 0.333$ and 0.400 there is an almost continuous variation of $h_i = Q_-$ from $q^* = Q_- = 0.333$ to 0.5 at $T^* = T_Q^*$. We call this the Q_- region. Between $x = 0.575$ and 0.625 the peaks first form flat plateaus without clearly showing satellite peaks (see Fig. 11). At low temperature $T^* = 0.05$ [Fig. 9(b)], the situation is more symmetric and shows a stabilization of $h_i = Q_- = 0.4$ and $h_i = Q_+ = 0.4$ (and 0.6), corresponding to an ortho-V phase, for $x = 0.4$ and 0.6. In a small region around that, these peaks are found in combination with the neighboring, ortho-III or ortho-II phases, respectively.

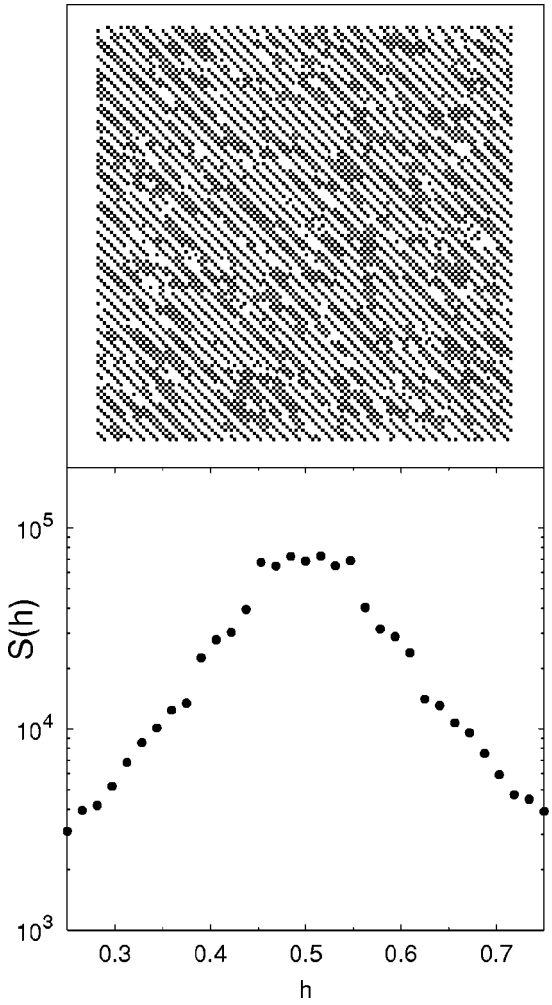

FIG. 11. A typical plateau peak and the corresponding structure, here at $T^* = 0.08$, $x = 0.425$, and $V_5 = 0.04V_1$. The width of the plateaus are indicated by the vertical bars in Figs. 9 and 10.

For the larger value $V_5 = 0.04V_1$ the behavior is similar, as shown in Fig. 10(c). However, there are also important differences. First we note that the T_Q^* phase boundary is depressed further, especially toward the ortho-II phase around $x = 0.5$, and that $Q_\pm$ regions become broader at the expense of the mixed-phase regions. The previously discussed gap between the tetragonal-ortho-I and the ortho-I-ortho-II transitions does become slightly larger; however, since both transition lines are severely depressed, the effect on the gap is not very large.

The q^* variation on the low-x side exhibits an almost continuous variation of Q_- between $q^* = 0.333$ and 0.5 for x

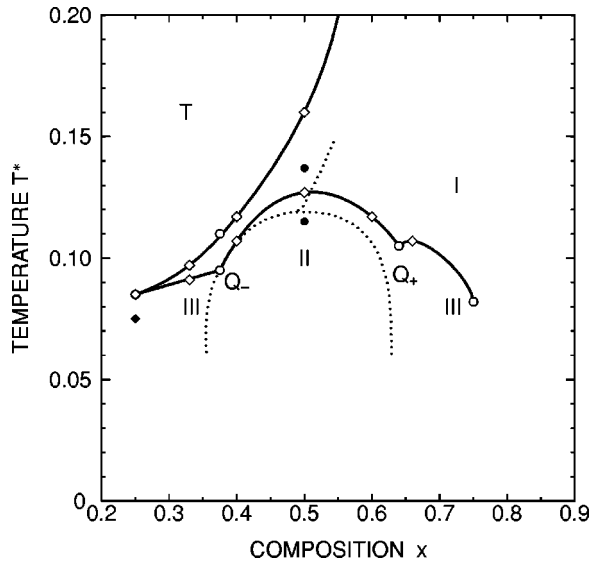

FIG. 12. Simulated 3D phase diagram for $V_4=-0.02V_1$ and $V_5=0.02V_1$ (open symbols). The full line is a guide to the eye. Closed symbols: $V_4=-0.01V_1$. Dotted line: the 2D simulation for $V_5=0$. We did not investigate the detailed ordering below the ortho-I to ortho-N phase line. Results for a 16-member ensemble of size $64\times64\times32$ are indicated by open and closed $\diamond$, while open and closed $\bigcirc$ indicate results for 16-member ensemble of size $128\times128\times32$.

between 0.333 and 0.425, with sign of mixed phase at $T^*=0.05$; see Figs. 10(a) and 10(b). On the high-x side this behavior is terminated when Q_+ approaches 0.550 by broad plateau peaks, one of which is shown in Fig. 11. The region with ortho-II order ($h_2=0.5$) is not surprisingly rather smaller than for $V_5=0.02V_1$.

V. RESULTS OF 3D SIMULATION

A small attractive interaction of oxygens occupying equivalent positions in neighboring planes is needed to account for an observed weak correlation along the c axis. The resulting phase diagram is shown in Fig. 12 mainly for $V_5=0.02V_1$ and $V_4=-0.02V_1$ (a value suggested by de Fontaine *et al.*[30]) Although less detailed, it is clearly very similar to that for $V_4=0$, Fig. 9. At $x=0.5$ the 3D simulations performed by Fiig *et al.*[39] with $V_5=0$ yield a gap of $\Delta T_G^*=0.03$. For $V_5=0.02V_1$, and $V_4=-0.02V_1$ we obtain a gap $\Delta T_G^*=0.033$ corresponding to $\Delta T_G\sim180$ K, which is approaching the experimental gap $\Delta T_{G,\,\mathrm{expt}}\sim250$ K. In order to demonstrate the general dependence on T_Q^* we have also made simulations for $V_4=-0.01V_1$ at $x=0.5$ and 0.25, indicated by full symbols.

The line shape for q^* in the l direction has, of course, a relatively low resolution. However, a rough analysis of the $V_4=-0.02V_1$ data shows that the shape, below the ordering temperature, is consistent with a Lorentzian to a power $\phi\sim1.5$. This applies to the peak at $(h,k,l)=(\frac{1}{2},0,0)$ in the interval $0.4<x<0.5$. It also applies to the peak at $(h,k,l)=(\frac{1}{3},0,0)$ in the interval $0.25<x<0.375$. The HWHM at the lowest simulated temperatures is $\Delta l^*\sim0.015$ (r.l.u.) at $T^*=0.05$ for $x=0.25$ and $\Delta l^*\sim0.010$ at $T^*=0.08$ for $x=0.5$. The ordering is weaker for larger x. In the interval $0.64<x<0.66$ the peak at $(\frac{1}{3},0,0)$ has $\Delta l^*\sim0.03$ at $T^*=0.09$, and $\phi\sim1.5$. Generally, Δl^* drops to a constant minimum at T_Q^*, as Δh^* and Δk^*. However, for $x=0.6$ we find an interesting, different behavior, shown in Fig. 13. At $T_Q^*=0.117$, Δh^* drops to a low value of 0.010, indicating extended short-range order along the a direction. This is independent of the order along the c direction, which remains very weak (and is actually corresponding to that found experimentally at $x=0.4$). At lower temperatures ($T^*\sim0.1$) the order along the c axis increases (Δl^*decreases). This occurs simultaneously with the development of signatures of mixed phases in the plane indicated by coexistence of the $(\frac{1}{2},0,0)$ peak and a $(Q_+,0,0)$ peak. For $V_4=-0.01V_1$ at $T^*=0.09$ and $x=0.5$ we find $\Delta l^*=0.015$ and $\phi\sim1.5$.

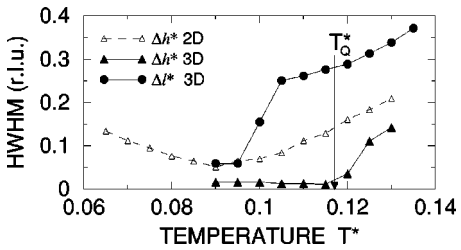

FIG. 13. The simulated HWHM at $x=0.6$ and $V_5=0.02V_1$. Filled symbols: 3D with $V_4=-0.02V_1$; open symbols: 2D. Note that Δl^* remains high through T_Q^*. For all other investigated x values Δl^* drops to a constant minimum as Δh^* and Δk^*. The 2D width increases at low temperature due to the development of two peaks.

The used 3D interaction parameters $|V_4|$ are probably too large, resulting in longer ranged ordering in the c direction than observed experimentally.[39] The smallness of the interplane coupling underpins the validity of the extensive 2D results. The ordering within the planes is extended in the 3D simulation for the used $V_4=-0.02V_1$, with signatures of long-range order for some ensemble members for the available sample size. This makes it difficult to determine the line shape in the h and k directions. For $x=0.4$ and $T^*=0.09$, $S(h)$ is consistent with a simple Lorentzian, i.e., with $\phi=1$. For $x=0.5$ and $T^*=0.08$ the line shape is consistent with having $1\leqslant\phi\leqslant1.5$.

VI. ANALYTIC RESULTS IN THE SPHERICAL APPROXIMATION

A shortcoming of the Monte Carlo method is that it is difficult and time consuming to explore a large part of the parameter space. Hence an approximate theory is valuable both for a deeper understanding of the results and for extrapolating them by exploring the general influence of various parameters. In Ref. 39 it was demonstrated that a generalization of the spherical model to Ising-type systems was possible, and yielded good results for the transition temperature compared with Monte Carlo and exact results. This amounts to a scaling of the mean field results in order to fulfil the exact spin length constraint, which can be written

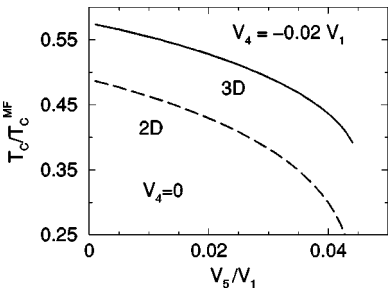

FIG. 14. The calculated reduction of T_c relative to the mean-field value as a function of V_5, in two and three dimensions.

$$G(R)=\frac{1}{N}\sum_{\mathbf{q}}\frac{1}{R-\mathcal{J}(\mathbf{q})/\mathcal{J}(\mathbf{Q})}=\frac{T_c^{\mathrm{MF}}}{T_c}. \tag{3}$$

It is clear that the reduction factor for T_c, $1/G(R)$, is very sensitive to the general behavior of the interaction surface $\mathcal{J}(\mathbf{q})$ in Fourier space, in particular for $\mathbf{q}\sim\mathbf{Q}$ when $R\to 1$.

For the ortho-I to ortho-II transition we have $\mathcal{J}(\mathbf{q})=2[V_2\cos(q_y)+V_3\cos(q_x)+V_4\cos(q_z)+V_5\cos(2q_x)]$, $\mathbf{Q}=(\pi,0,0)$, using the convention from Ref. 39. The mean-field transition temperature is, assuming predominant occupation, $x-\epsilon$, of sublattice a with chains in the $a(y)$-direction, and only a small occupation ϵ on the sublattice b with chains in the $b(x)$ direction, given by[39] $T_c^{\mathrm{MF}}(\text{I-II})=\mathcal{J}(\mathbf{Q})(x-\epsilon)(1-x+\epsilon)$ for the composition x close to $x=1/2$. The parameter $R=1+\Delta$ at the transition temperature is determined by fitting to the Monte Carlo T_c for the 2D ASYNNNI model (at $x=0.5$ and with $V_4=V_5=0$). This yields simultaneously, in comparison with simpler Ising models, an agreement within 6% of the exact 2D nearest-neighbor (NN) Ising T_c and within 0.5% agreement with the best Monte Carlo determination of T_c for the 3D NN Ising model.[46] Δ is found[39] to have the value $\Delta=0.0216$. It represents the fact that it costs a finite energy to create the lowest energy excitation in an Ising-type system, corresponding to the Goldstone mode for Heisenberg systems. Because of this finite gap, the sum—or corresponding triple integral—can in fact be performed directly. A more elegant method is to use the reduction into a single integral over an elliptic function by Morita and Horiguchi[47] and generalized in Ref. 39,

$$G(R)=\frac{8\pi}{\sqrt{\gamma\beta}}\int_0^{\pi}k\,K(k^2)dx, \tag{4}$$

where $K(k^2)$ is the complete elliptic integral of the first kind (See Ref. 48), and k now equals

$$k=\left[\frac{4\beta\gamma}{\left(R-\sum_n\alpha_n\cos nx\right)^2-(\beta-\gamma)^2}\right]^{1/2}, \tag{5}$$

where the normalized interaction constants are $\alpha_1=2V_3/\mathcal{J}(\mathbf{Q})$, $\beta=2V_2/\mathcal{J}(\mathbf{Q})$, $\gamma=2V_4/\mathcal{J}(\mathbf{Q})$, and $\alpha_2=2V_5/\mathcal{J}(\mathbf{Q})$, and we have assumed $\alpha_{n>2}=0$. Figure 14 shows the influence on T_c(I-II) by the introduction of V_5.

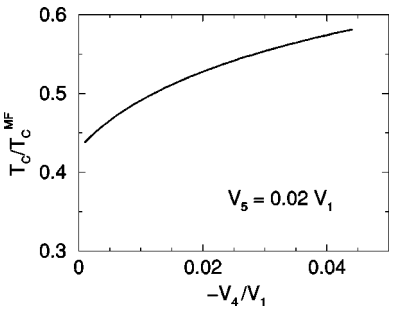

FIG. 15. The calculated reduction of T_c relative to the mean-field value as a function of the 3D interaction V_4, at a fixed value of $V_5=0.02V_1$.

Very good agreement is obtained with the transition temperatures found in the Monte Carlo studies for both two and three dimensions with $|V_4|=0.02|V_1|$. The additional repulsive interaction V_5 increases the frustration effects and fluctuations and hence decreases T_c/T_c^{MF} significantly. This is probably the explanation of why no Bragg peaks appear in the simulations or experiments. A test shows that we obtain identical results using Eqs. (3) and (4). Figure 15 shows the effect of a 3D coupling $V_4\neq 0$ upon a model which contains a finite $V_5=0.02V_1$. Again a strong effect, much larger than the simple linear modification that the addition of parameters cause in the mean field T_c^{MF}.

Using integral (4) we can easily estimate the effect on T_c(I-II) of possible further interactions with oxygens on more distant chains. Suppose we include a complete screened Coulomb interaction of the form $\alpha_r=\alpha\exp(-\kappa r)/r$ in Eq. (5). For $\alpha=V_3^2/[\mathcal{J}(\mathbf{Q})V_5]$ and $\kappa=\ln(V_3/2V_5)$ we obtain the first two interactions V_3 and V_5 as before, which gave $T_c(\text{I-II})_{3,5}=0.127|V_1|$ for $V_3=0.12V_1$ and $V_5=0.02V_1$. The new scale factor $\tilde{\mathcal{J}}(\mathbf{Q})=\mathcal{J}(\mathbf{Q})(1+f)$ now needed in Eq. (3) includes the contribution from the infinite tail: $f=2\Sigma_{n=3}^{\infty}(-1)^n\alpha\exp(-\kappa n)/n/\mathcal{J}(\mathbf{Q})$. However, if in Eq. (5) we instead scale $R\to R(1+f)$ the constants $\alpha_1,\alpha_2,\beta,\gamma$ as well as T_c^{MF}(I-II) are the same as above. The result at $x=0.5$ is $T_c(\text{I-II})_{\text{Screened Coulomb}}=0.137|V_1|/k_B$. We can also consider a more slowly decaying interaction of the form $\alpha_r=\alpha\exp(-\kappa r)$ representing the total interaction of oxygens on correlated chains. For $\alpha=2V_3^2/[\mathcal{J}(\mathbf{Q})V_5]$ and $\kappa=\ln(V_3/V_5)$ we obtain the first two interactions V_3 and V_5 as before and $f=2\Sigma_{n=3}^{\infty}(-1)^n\alpha\exp(-\kappa n)/\mathcal{J}(\mathbf{Q})$. The result for $x=0.5$ is $T_c(\text{I-II})_{\text{Exp. decay}}=0.135|V_1|/k_B$. In both cases the changes are small and increase T_c(I-II) slightly toward the mean field $T_c^{\mathrm{MF}}(\text{I-II})=0.24|V_1|$, as expected for long-range interactions. However, the effect on T_c(I-II) of the tails can easily be included in an effective value for V_5, as used in the MC calculations. In the above evaluation we have used the exact results[48]

$$\sum_{n=1}^{\infty}\frac{e^{-\kappa n}}{n}\cos nx=\ln\left\{\frac{1}{\sqrt{1-2e^{-\kappa}\cos x+e^{-2\kappa}}}\right\}, \tag{6}$$

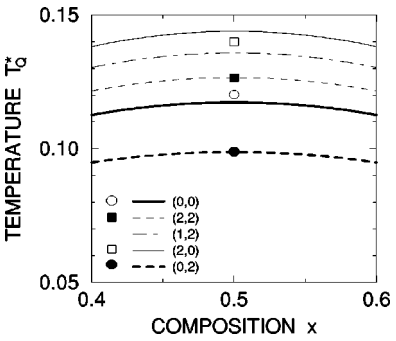

FIG. 16. The calculated T_Q^* as a function of x for various values of the parameters. These are indicated as the sets (m,n), where $(-V_4,V_5)=0.01V_1(m,n)$. The symbol values are from the Monte Carlo simulations; open and closed circle: two dimensions; open and closed box: three dimensions.

$$\sum_{n=1}^{\infty} e^{-\kappa n}\cos nx = e^{-\kappa}\frac{\cos x - e^{-\kappa}}{1-2e^{-\kappa}\cos x + e^{-2\kappa}}. \qquad (7)$$

The variation with x around 0.5 is shown on Fig. 16, neglecting ϵ for clarity, for the parameter choices used in the Monte Carlo simulation. The agreement is good at $x=0.5$. The effect of a finite ϵ is to shift the maximum transition temperature to $x>0.5$. This effect is clearly seen in the Monte Carlo results, cf. Figs. 9 and 10.

The above scaling correction of T_c^{MF} can of course not be expected to remain valid near the percolation limit in the dilute systems, where the long-range order disappears. This was demonstrated for T_c(I-II) by comparison with 2D and 3D simulations with $V_5=0$.[39]

At the tetragonal to ortho-I transition, T_c(T-I), the symmetry is broken between equal populations of the sublattices a and b. A similar estimate can be made using Eq. (3) with $\mathcal{J}'(\mathbf{q})=[\mathcal{J}(\mathbf{q})+\mathcal{J}(\hat{\mathbf{q}})]/2+4V_1\cos(q_x/2)\cos(q_y/2)$, where $\hat{\mathbf{q}}=(q_y,q_x,q_z)$, $\mathbf{Q}=(2\pi,0,0)$, and $T_c^{\mathrm{MF}}(\text{T-I})=\mathcal{J}'(\mathbf{Q})(x/2)\times[1-(x/2)]=0.84|V_1|$ for $V_4=-0.02V_1$ and $V_5=-0.02V_1$. It yields a substantial reduction: $T_c(\text{T-I})=0.56T_c^{\mathrm{MF}}(\text{T-I})$. Although the reduction factor is similar to that for the ortho-I to ortho-II transition, it is not sufficient and gives a T_c(T-I) about a factor of 4 larger than obtained in the Monte Carlo simulations. We believe the reason for this is that for the T-I transition we are, at $x\sim0.5$, too close to the percolation limit for the ortho-I order. This is corroborated by the fact that the x dependence of $T_c(x)$(T-I) shows about twice as large a slope as can be obtained from a rigid scaling of $T_c^{\mathrm{MF}}(x)$(T-I) near $x\sim0.5$

The above way of including the fluctuation correction to the mean-field behavior gives surprisingly good results in a large number of cases, as demonstrated. The failure of the description of the T-I transition, shows that this transition must be very strongly fluctuation or dilution depressed. An inspection of the snapshots obtained from the MC simulations reveals, that the structure just above T_c(T-I) does not have a random a and b occupation, as presumed in the most simple mean field theory, yielding the above $T_c^{\mathrm{MF}}(x)$(T-I). Rather, the overall symmetry is retained, but broken locally by the formation of many small dilutely populated, but pure a and b domains, the size of which strongly depends on x and T. At the transition one of these starts to dominate.

This means that the tetragonal to ortho-I transition is very sensitive to details in the model. It may explain the fact that in experiments the gap between the T-I and I-II transitions is found to be somewhat larger than can be obtained by the extended ASYNNNI model, including a finite V_5, as demonstrated below.

VII. THEORETICAL MODELS FOR THE ORDERING

How can one understand the regions $Q_\pm$ which exhibit pseudo continuous variation of the ordering vector Q, shown in Figs. 9(a) and 10(a). Khachaturyan and Morris[49] made a simple model and a corresponding theory that rather closely accounts for this behavior. It described the diffuse scattering from Magneli-type random faulting of long (infinite) oxygen chains (or actually planes), where only narrow antiphase boundaries are allowed. This results in the interesting prediction that the ''ortho-II'' peak, regarded as a broad peak centered at $h_2=0.5$, is stable from $x=0.5$ up to $x=0.556$. Then the peak should split with a splitting going continuously toward 0.333 at $x=0.667$, indicated as the dashed lines in Figs. 9(a) and 9(b) and 10(a) and 10(b). Clearly, the prediction follows roughly the results of the simulation. It is remarkable that all that is assumed in the model is a repulsion between neighboring defects, and otherwise no interaction. Reference 49 discussed the region $\frac{1}{2}\leqslant x\leqslant\frac{2}{3}$. However, our data show that this may apply for $\frac{1}{3}\leqslant x\leqslant\frac{1}{2}$ as well.

We believe our restricted range model, enforced by introducing a finite V_5, is indeed sufficient to account for this important feature, and that no new qualitative phenomena would be found by including further ranged interactions in the temperature range considered. The theory was criticized by de Fontaine and Moss,[50] in particular with respect to the picture described requiring planar Magneli defects of infinite extent. We see from our real-space snapshots that the above assumed idealized picture by no means is needed to produce results for the diffuse scattering as predicted by Khachaturyan and Morris, although the random faulting picture probably is close to the actual reality. If we were to assume the simpler de Fontaine model,[29] which only assumes repulsion (of any range) between any chains of oxygen ions, one would expect an almost linear approach from $q^*=\frac{1}{2}$ toward $q^*=\frac{1}{3}$ with possible $Q_\pm$ phases of so-called ''structure combination branching'' on larger real space scale, and hence not showing the stabilized region of $q^*=0.5$ around $x=0.5$. Such large-scale superstructures are only expected at low temperatures, but have not been observed beyond the ortho-VIII phase. We believe our extended ASYNNNI model with $V_5=0.02V_1$ does give a realistic picture of the real-space oxygen ordering in YBCO. The theory of Khachaturyan and Morris accounts quite well for the q^* variation at low T^*, and in fact also for the symmetric case for $x<\frac{1}{2}$; however, the picture they advanced as their basis is much more restricted, and hence unphysical, than needed. Clearly, small domains of rather mixed order regions are sufficient to produce the diffuse scattering they predict. Further, their simple

model was of course not designed to describe the mixed phases for which we have found evidence. Another difference is that the broad diffuse line shape they predicted for $\frac{1}{2}<x<\frac{5}{9}$ is rather too simple and appears with a more flat top; see Fig. 11. It reduces to a Lorentzian-raised-to-a-power for $x=0.5$. We have previously studied diffuse scattering in similar simplified linear models in which we have described the line shape as a function of possible distributions of nonoverlapping antiphase domains.[39,51] The model of Khachaturyan and Morris constitutes a particular case of that; hence the line shape is in the same class.

Discussion of dynamical effects and nonequilibrium behavior

In experimental investigations[17] it was shown that the determined pseudo-ordered structure found in various samples depends on the history of the sample. It is thus possible, by very long and specially designed annealing schemes, to obtain a structure chacterized by larger domains at a given low temperature, than if a fast quench to the same temperature is performed. In the simulations we similarly find transitions which are not characterized by the development of Bragg peaks, but rather only by a rapid decrease of the width and an increase of the intensity of diffuse, short-range order peaks. We have tested that the corresponding domain structure does not depend strongly on the way we cool through T_c^*. For example, the same structure is obtained by standard stepwise cooling from a relatively high $T^*>T_c^*$(T-I) in equidistant steps of $\Delta T^*=0.05$ as is obtained after a direct quench from a very high $T^*\gg T_c^*$(T-I) to slightly below T_c^*(I-II), and then allowing the system to develop from there. At lower temperatures the system often develops into stripe phases. This is not the equilibrium single-domain structure, but because of periodic boundaries the structures are frozen in a metastable multidomain state. Since the calculated and measured structure factors are very similar, we believe the simulated real-space patterns also correspond to the actual oxygen ordering in the planes when taking into account the observed scale.

Analyses of the simulated 3D structures reveal that there is an almost perfect ordering (at low T^*) of the structure in adjacent planes in slabs of several planes thickness. Then, abruptly, an ordering of alternative domains sets in, and may prevail for the next couple of planes. In other words, the simulations produce a pronounced slab structure stacked along the *c* direction. Similar slab structures are found in the plane, in particular in the *a* direction. Simultaneously, the line shape develops into a Lorentzian to a power $\phi\neq 1$.

In order to interpret this we have made a simple 1D model with two space filling alternative domains: an in-phase domain with a scattering length of $f(r)=1$, at layer r and an out-of-phase-domain with a scattering length at layer r' of $f(r')=-1$. The thickness or length L of the slabs are assumed to be distributed exponentially, $D(L)=\exp(-\kappa L)$, with an average length $\langle L\rangle$ (in units of lattice constants). The analytic result for this case was considered by Fiig *et al.*[52] The Fourier transform is a perfect Lorentzian with a HWHM of Δ^*, plus a background. However, the half width is related to the average length as $\langle L\rangle=1/(\pi\Delta^*)$ lattice constants [i.e., not $1/(2\pi\Delta^*)$ as for the dilute case] for Δ^* in reciprocal-lattice units. As a test, a simple model calculation was performed for an exponential distribution of slab thicknesses with average $\langle L\rangle=1/\kappa=8$, and a (periodic) sequence with total length 800, and using 2000 different members in the ensemble. Using the half width of the line shape one obtains $1/(\pi\Delta^*)=7.97$, in agreement with the direct evaluation from the sequences and the analytic result.[52] The reason it is slightly smaller than 8 is that in the finite length model distribution there is not quite sufficiently many very very thick slabs.

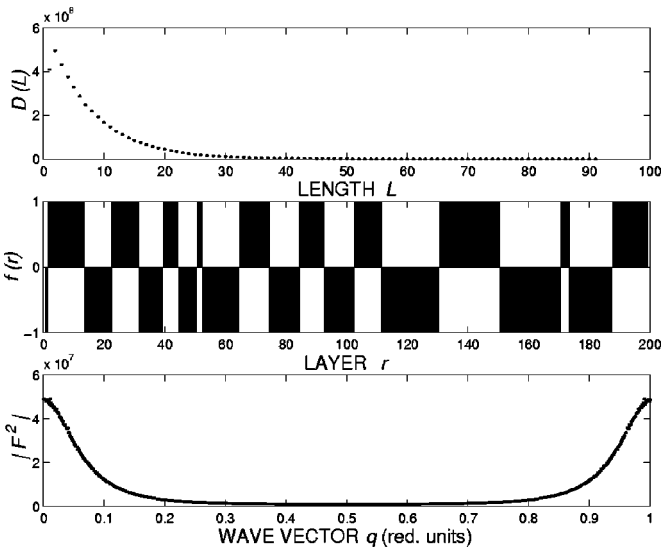

FIG. 17. Slab model and the corresponding structure factor. Top: the distribution function $D(L)=\exp(-\kappa L)$, $\kappa=1/8$, except for $L=1$, where it is reduced by 25%. This yields the average $\langle L\rangle=8.16$. Middle panel: a corresponding, typical array of slabs with alternating scattering length $f(r)$. Lower panel: the resulting line shape of the Fourier transform $|F(q^*)|^2$ in reciprocal lattice units. It is clearly not Lorentzian, but it can be perfectly fitted to a Lorentzian to a power $\phi=1.36$.

In Ref. 52 the distribution $D(L)$ which gives rise to the Lorentzian-squared line shape was derived for the dilute case. It shows that a decrease of the probability of the narrowest slabs is all what is needed to provide that line shape. Based on this conclusion we reduced the probability of the presence of a single isolated layer in the exponential distribution (see Fig. 17, top panel). The middle panel shows part of a typical distribution of slabs. The picture is clearly dominated by slabs around the directly calculated average thickness $\langle L\rangle=8.16$. The absolute square Fourier transform $|F(q^*)|^2$ of an ensemble of 10000 such randomly different sequences is shown at the bottom. (Clearly, to demonstrate these effects with a similar number of independent Monte Carlo simulations is outside numerical possibilities.) A perfect fit to the resulting line shape can be made with a Lorentzian to the power ϕ, where $\phi=1.36$ when, as shown, the probability of finding a single layer is reduced by 25%. If it is reduced by 50%, the fit is perfect with a power $\phi=1.86$.

However, the relation between the HWHM (Δ^*) and κ, and in particular the average length, is now more complicated. For a Lorentzian raised to a power ϕ for a space filling distribution of domains, for which $S(q^*)=1/[(2\kappa)^2$

$+q^{*2}]^{\phi}$, one finds that $2\pi\Delta^*=2\kappa\{2^{1/\phi}-1\}^{1/2}$. But the average length is underestimated using κ determined directly as above. For the distribution yielding the Lorentzian-squared ($\phi=2$), one finds,[52] for $\kappa=1/8$, that the average length is twice as large as $1/\kappa$. For the line shape in Fig. 17 with $\phi=1.36$, we find $\Delta^*=0.0735$. If we naively use the HWHM to determine the average slab thickness as $1/(\pi\Delta^*)$, we would obtain $\langle L\rangle_{\mathrm{HWHM}}=4.33$. This is incorrect. It is only about half of the actual thickness of $\langle L\rangle=8.16$ directly determined from the distribution.

Both experimentally and in simulations, it is observed that the linewidth does not change significantly below T_Q^*, whereas ϕ increases toward $\phi=1.5$ near $x=0.5$, see Fig. 5. The above analysis indicates that this is a signature of a disappearance of the thinnest slabs, simultaneously with an increase in the average thickness of about a factor of 2. Without a knowledge of the actual distribution functions, it is not possible to make a more precise statement.

The above interpretation of deviations from Lorentzian line shape is quite different from the Porod argument, which arises when assuming a random distribution of equal size (low density) circular or spherical domains, a picture not supported by the simulations. The domain structure in the simulations is similar to the above assumed space-filling box model, and this gives structure factors in agreement with experiments. Therefore, we conclude the Porod model is not likely to be relevant for YBCO, which rather has stripelike and slablike domain structures, as can be seen in the simulated snapshots. Because the YBCO domains are box shaped, an integration in one direction (i.e., the l direction) does not change the line shape and hence the exponent ϕ. We can conclude that both our 2D and 3D simulations are in agreement with the experimentally found line shape with exponent $\phi_{\mathrm{expt}}=1.45\pm0.06$ for $x=0.5$. The line shape and the deviations from a Lorentzian shape is not a unique indicator of the local structure. The domain structure of YBCO is most likely not given by simple models, but is similar to that demonstrated by the snap-shots obtained by the present simulations.

The experimentally determined HWHM (Ref. 13) at room temperature ($T^*=0.055$) are $\Delta h^*=0.050$, $\Delta k^*=0.022$, $\Delta l^*=0.26$ in reciprocal-lattice units, for $x=0.4$. The line shape is not Lorentzian, but has $\phi>1$. This is, following the above analysis, consistent with boxlike domains with the average dimensions of about $(10a\times30b\times2c)$. At $x=0.5$ the average length in the a direction is $15a$ at $T=375$ K, increasing to $\sim30a$ at lower temperatures; cf. Fig. 5. Such domain sizes can easily be fitted into the twin domain structure, which is caused by strain effects. This substructures the crystals in perpendicular a and b domains on a mesoscale about ten times larger. Experimentally it is found for $x=0.5$, that the linewidth, and hence the degree of ordering, depends on the purity of the sample and the sample preparation. The more perfect samples have larger short-range ordering. For other x values we expect this dependence to be smaller because of the inherent oxygen disorder. The relative size of the short range order at the various x values may be judged from the line widths obtained in the simulations; see Fig. 1.

VIII. CONCLUSION

With the introduction of *one* extra in-plane parameter, the ASYNNNI model, thus extended, is able to explain several experimentally observed properties of the oxygen ordering in $YBa_2Cu_3O_{6+x}$ that the original ASYNNNI model is unable to account for. In this work it is demonstrated that this remains true when a 3D interactions and other interactions are also included. The general influence on T_c^*(I-II) of the value of the introduced new parameters V_4 and V_5 is calculated analytically and numerically using a generalization of the spherical approximation to apply to the extended ASYNNNI model. The introduced extra parameter $V_5=0.02V_1$ is optimal in explaining experimental observations, and is in accord with the estimated interaction, based on a screened Coulomb potential, whereas $V_5=0.04V_1$ is too large. The effect on T_c^*(I-II) of possible interactions to more distant neighbors is calculated using the spherical approximation. The effect is small and can be included in effective values for V_5. Their effect on the structures can be neglected because it would occur at such low temperatures that the slowing down of the oxygen diffusion prevents a realization in $YBa_2Cu_3O_{6+x}$, as already discussed by de Fontaine *et al.*[29]

We conclude, in agreement with Ref. 1, that the present simple fixed parameter model does account for most of the observed short-range order phenomena. This indicates that the inherent disorder in the oxygen structure, which is always observed in $YBa_2Cu_3O_{6+x}$, may not be driven by the electron transfer between the CuO_x and CuO_2 planes. More simply, we suggest that the variation in the copper valence is dictated by the disorder given by the oxygen interactions in $YBa_2Cu_3O_{6+x}$. This conclusion is in agreement with the lack of experimental evidence[17] for the predicted peak splitting as a consequence of a finite chain length distribution.[20] We do not claim that the effective parameters V_n are strictly independent of T and x, only that qualitative effects of this would be still more difficult to find in the structural data. The present study gives a more direct insight into the chain length distribution than the count of various valence Cu ions obtained by NMR experiments.[18]

The simulated phase diagram of ordering versus oxygen filling x and temperature is in good agreement with the experimental observations for $x\geqslant0.4$. In the model a fairly symmetrical behavior is found for $x<0.5$ and $x>0.5$. However, in the experiments the intensity becomes too weak to allow the observation of any sign of order for $x<0.35$. It should be pointed out that the simulations can account for some but not all of the gap between the onset of the ortho-I and ortho-II order, as observed at $x=0.5$. Theory and simulation indicate that the large gap is related to very strong correlation effects in and between patches of parallel and perpendicular chains. This is not fully understood, and provides an interesting challenge for further theory or simulations.

The domain structure is found to be roughly boxlike, in particular in the directions perpendicular to the chains, i.e., along the a and c axes, and with a more diffuse termination along the chains (b direction). Based on the understanding obtained in the present work and the experimentally determined line widths and shapes at $x=0.4$,[13] the domains in

$YBa_2Cu_3O_{6+x}$ at low temperatures are estimated to have average dimensions of $(10a \times 30b \times 2c)$. We have found agreement between the simulated and measured line shapes at temperatures where oxygen diffusion becomes very slow. This makes it plausible that the corresponding simulated real space snapshots represent the actual oxygen order relevant for the $YBa_2Cu_3O_{6+x}$ materials. Because of the slow diffusion this should also apply at lower temperatures, and hence even to the superconducting phase. A simple theory, based on scattering from boxlike domains with a broad size distribution, accounts for the deviations from the Lorentzian line shape. This is radically different from the Porod model. The physical basis for this is not supported for $YBa_2Cu_3O_{6+x}$ according to the simulations,

ACKNOWLEDGMENTS

We acknowledge SNF Grant No. 9602489 at UNI-C. D.M. would like to acknowledge the hospitality of Edinburgh Parallel Computing Center as a visitor sponsored by EU-TMR under Contract No. ERBFMGECT950051.

[1] D. Mønster, P.-A. Lindgård, and N.H. Andersen, Phys. Rev. B **60**, 110 (1999).
[2] G. Uimin, Int. J. Mod. Phys. B **6**, 2291 (1992).
[3] J. Zaanen, A. Paxton, O. Jepsen, and O.K. Andersen, Phys. Rev. Lett. **60**, 2685 (1988).
[4] W.E. Pickett, R.E. Cohen, and H. Krakauer, Phys. Rev. B **42**, 8764 (1990).
[5] J.D. Jorgensen, S. Pei, P. Lightfood, H. Shi, A.P. Paulikas, and B.W. Veal, Physica C **167**, 571 (1990).
[6] H.F. Poulsen, N.H. Andersen, J.V. Andersen, H. Bohr, and O.G. Mouritsen, Phys. Rev. Lett. **66**, 465 (1991).
[7] H.F. Poulsen, N.H. Andersen, J.V. Andersen, H. Bohr, and O.G. Mouritsen, Nature (London) **349**, 594 (1991).
[8] D.J. Werder, C.H. Chen, R.J. Cava, and B. Batlogg, Phys. Rev. B **38**, 5130 (1988).
[9] M.A. Alario-Franco, C. Chaillout, J.J. Capponi, J. Chenavas, and M. Masezio, Physica C **156**, 455 (1988).
[10] J. Reyes-Gasga, T. Krekels, G. Van Tendeloo, J. Van Landuyt, W.H.M. Bruggink, M. Verweij, and S. Amelincks, Solid State Commun. **71**, 269 (1989).
[11] R. Beyers, B.T. Ahn, G. Gorman, V.Y. Lee, S.S.P. Parkin, M.L. Ramirez, K.P. Roche, J.E. Vazquez, T.M. Gur, and R.A. Higgins, Nature (London) **340**, 619 (1989).
[12] R.M. Fleming, L.F. Schneemeyer, P.K. Gallaghan, B. Batlogg, L.W. Rupp, and J.V. Waszczak, Phys. Rev. B **37**, 7920 (1988).
[13] T. Zeiske, R. Sonntag, D. Hohlwein, N.H. Andersen, and T. Wolf, Nature (London) **353**, 542 (1991).
[14] V. Plakhty, A. Stratilatov, Y. Chemenenkov, V. Fedorov, S.K. Sinha, C.K. Loong, B. Gaulin, M. Vlasov, and S. Moshkin, Solid State Commun. **84**, 639 (1992).
[15] P. Schleger, R.A. Hadfield, H. Casalta, N.H. Andersen, H.F. Poulsen, M. von Zimmermann, J.R. Schneider, R. Liang, P. Dosanjh, and W.N. Hardy, Phys. Rev. Lett. **74**, 1446 (1995).
[16] P. Schleger, H. Casalta, R.A. Hadfield, H.F. Poulsen, M. von Zimmermann, N.H. Andersen, J.R. Schneider, R. Liang, P. Dosanjh, and W.N. Hardy, Physica C **241**, 103 (1995).
[17] N.H. Andersen, M. von Zimmermann, T. Frello, M. Käll, D. Mønster, P.-A. Lindgård, J. Madsen, T. Niemöller, H.F. Poulsen, O. Schmidt, J.R. Schneider, T. Wolf, P. Dosanjh, R. Liang, and W.N. Hardy, Physica C **317-318**, 259 (1999).
[18] H. Lütgemeier, S. Schmenn, P. Meuffels, O. Storz, R. Schöllhorn, Ch. Niedermayer, I. Heinmaa, and Yu. Baikov, Physica C **267**, 191 (1996).
[19] D.J. Liu, T.L. Einstein, P.A. Sterne, and T.L. Wille, Phys. Rev. B **52**, 9784 (1995).
[20] G. Uimin, Phys. Rev. B **50**, 9531 (1994).
[21] H. Haugerud, G. Uimin, and W. Selke, Physica C **275**, 93 (1997).
[22] A.A. Aligia, A.G. Roja, and B.R. Alascio, Phys. Rev. B **38**, 6604 (1988).
[23] A.A. Aligia, J. Garcés, and H. Bonadeo, Phys. Rev. B **42**, 10 226 (1990).
[24] A.A. Aligia, Europhys. Lett. **18**, 181 (1992).
[25] A.A. Aligia, Phys. Rev. B **47**, 15 308 (1993).
[26] A.A. Aligia and J.M. Eroles, Physica C **272**, 197 (1996).
[27] A.A. Aligia, S. Koval, and R. Migoni, Phys. Rev. B **57**, 1241 (1998).
[28] D. de Fontaine, L.T. Wille, and S.C. Moss, Phys. Rev. B **36**, 5709 (1987), ASYNNNI stands for the asymmetric next-nearest-neighbor Ising model.
[29] D. de Fontaine, G. Ceder, and M. Asta, Nature (London) **343**, 544 (1990).
[30] D. de Fontaine, G. Ceder, and M. Asta, J. Less Common Met. **164-165**, 108 (1990).
[31] V.E. Zubkus, S. Lapinskas, and E.E. Turnau, Physica C **159**, 501 (1989).
[32] V.E. Zubkus, S. Lapinskas, and E.E. Turnau, Physica C **166**, 472 (1990).
[33] V.E. Zubkus, E.E. Turnau, S. Lapinskas, and P.J. Kundrotas, Phys. Rev. B **43**, 13112 (1991).
[34] V.E. Zubkus, P.J. Kundrotas, and A.S. Orliukas, J. Phys. C **4**, 83 (1992).
[35] V.E. Zubkus, S. Lapinskas, A. Rosengren, and E.E. Turnau, Physica C **206**, 155 (1993).
[36] G. Ceder, M. Asta, and D. de Fontaine, Physica C **177**, 106 (1991).
[37] S. Semenovska and A.G. Khachaturyan, Phys. Rev. B **46**, 6511 (1992).
[38] T. Fiig, N.H. Andersen, J. Berlin, and P.-A. Lindgård, Physica C **217**, 34 (1993).
[39] T. Fiig, N.H. Andersen, P.-A. Lindgård, J. Berlin, and O.G. Mouritsen, Phys. Rev. B **54**, 556 (1996).
[40] N.H. Andersen, B. Lebech, and H.F. Poulsen, Physica C **172**, 31 (1990).
[41] In a previous study (Ref. 39) we investigated the effect of extending the ASYNNNI model with a 3D attractive interaction $V_4 = -0.02V_1$ between neighboring CuO_x planes.

[42] P.A. Sterne and L.T. Wille, Physica C **162-164**, 223 (1989).
[43] S. Mannsteadt and G.S. Pawley, Phys. Rev. B **62**, 4169 (2000).
[44] T. Castán and P.-A. Lindgård, Phys. Rev. B **40**, 5069 (1989); T. Castán and P.-A. Lindgård, *ibid.* **41**, 4659 (1990).
[45] P.-A. Lindgård, H.V. Virtiö, and O.G. Mouritsen, Phys. Rev. B **38**, 6798 (1988).
[46] C. Baillie, R. Gupta, K. Hawick, and G.S. Pawley, Phys. Rev. B **45**, 10 438 (1992).
[47] T. Moriyta and T. Horiguchi, J. Math. Phys. **6**, 981 (1971).
[48] *Handbook of Mathematical Functions*, edited by M. Abramowitz and I.A. Stengun (Dover, New York, 1972).
[49] A.G. Khachaturyan and J.W. Morris Jr., Phys. Rev. Lett. **64**, 76 (1989).
[50] D. de Fontaine and S.C. Moss, Phys. Rev. Lett. **67**, 527 (1991).
[51] G. Uimin and P.-A. Lindgård, Acta Crystallogr., Sect. A: Found. Crystallogr. **53**, 15 (1997).
[52] T. Fiig, N.H. Andersen, J. Berlin, and P.-A. Lindgård, Phys. Rev. B **51**, 12246 (1995). In the text and in Table I of that paper, by mistake the full width at half maximum (FWHM) is indicated. This should be the HWHM.